Antireflective property of thin film a-Si solar cell structures with graded refractive index structure

Sung Jun Jang,[1] Young Min Song,[1] Chan Il Yeo,[1] Chang Young Park,[1] Jae Su Yu,[2] and Yong Tak Lee[1,3,4,*]

[1]School of Information and Communications, Gwangju Institute of Science and Technology, 1 Oryong-dong, Buk-gu, Gwangju, 500-712, South Korea

[2]Department of Electronics and Radio Engineering, Kyung Hee University,1 Seocheon-dong, Giheung-gu, Yongin-si, Gyeonggi-do, 446-701, South Korea

[3]Graduate Program of Photonics and Applied Physics, Gwangju Institute of Science and Technology, 1 Oryong-dong, Buk-gu, Gwangju, 500-712 South Korea

[4]Department of Nanobio Electronics and Materials, Gwangju Institute of Science and Technology,1 Oryong-dong, Buk-gu, Gwangju, 500-712, South Korea

**ytlee@gist.ac.kr*

Abstract: We report the antireflective property of thin film amorphous silicon (a-Si) solar cell structures based on graded refractive index structure together with theoretical analysis. Optimizations of the index profile are performed using the rigorous coupled-wave analysis method. The graded refractive index structure fabricated by oblique angle deposition suppresses optical reflection over a wide range of wavelength and incident angle, compared to the conventional structure. The average reflectance of thin film a-Si solar cell structure with the graded refractive index structure is suppressed by 54% at normal incidence due to the effective refractive index matching between ITO and a-Si, indicating a reasonable agreement with calculated results.

OCIS codes: (040.5350) Photovoltaic; (160.4760) Optical properties; (310.1210) Antireflection coatings; (310.1860) Deposition and Fabrication; (310.4165) Multilayer design.

References and links

1. D. E. Carlson, and C. R. Wronski, "Amorphous silicon solar cell," Appl. Phys. Lett. **28**(11), 671–673 (1976).
2. A. V. Shah, H. Schade, M. Vanecek, J. Meier, E. Vallat-Sauvain, N. Wyrsch, U. Kroll, C. Droz, and J. Bailat, "Thin-film silicon solar cell technology," Prog. Photovolt. Res. Appl. **12**(23), 113–142 (2004).
3. K. L. Chopra, P. D. Paulson, and V. Dutta, "Thin-film solar cells: An overview," Prog. Photovolt. Res. Appl. **12**(2–3), 69–92 (2004).
4. M. A. Green, "Lambertian light trapping in textured solar cells and light-emitting diodes: analytical solution," Prog. Photovolt. Res. Appl. **10**(4), 235–241 (2002).
5. Lord Rayleigh, "On reflection of vibrations at the confines of two media between which the transition is gradual," Proc. London Math. Soc. **s1–11**(1), 51–56 (1879).
6. Y. F. Huang, S. Chattopadhyay, Y. J. Jen, C. Y. Peng, T. A. Liu, Y. K. Hsu, C. L. Pan, H. C. Lo, C. H. Hsu, Y. H. Chang, C. S. Lee, K. H. Chen, and L. C. Chen, "Improved broadband and quasi-omnidirectional anti-reflection properties with biomimetic silicon nanostructures," Nat. Nanotechnol. **2**(12), 770–774 (2007).
7. Y. M. Song, J. S. Yu, and Y. T. Lee, "Antireflective submicrometer gratings on thin-film silicon solar cells for light-absorption enhancement," Opt. Lett. **35**(3), 276–278 (2010).
8. J. Y. Chyan, W. C. Hsu, and J. A. Yeh, "Broadband antireflective poly-Si nanosponge for thin film solar cells," Opt. Express **17**(6), 4646–4651 (2009).
9. Y. J. Lee, D. S. Ruby, D. W. Peters, B. B. McKenzie, and J. W. P. Hsu, "ZnO nanostructures as efficient antireflection layers in solar cells," Nano Lett. **8**(5), 1501–1505 (2008).
10. S. Chhajed, M. F. Schubert, J. K. Kim, and E. F. Schubert, "Nanostructured multilayer graded-index antireflection coating for Si solar cells with broadband and omnidirectional characteristics," Appl. Phys. Lett. **93**(25), 251108 (2008).
11. W. Qiu, Y. M. Kang, and L. L. Goddard, "Quasicontinuous refractive index tailoring of SiN_x and SiO_xN_y for broadband antireflective coatings," Appl. Phys. Lett. **96**(14), 141116 (2010).
12. X. Li, J. Gao, L. Xue, and Y. Han, "Porous polymer films with gradient-refractive-index structure for broadband and omnidirectional antireflection coatings," Adv. Funct. Mater. **20**(2), 259–265 (2010).
13. S. J. Jang, Y. M. Song, J. S. Yu, and Y. T. Lee, "Structural and optical properties of silicon by tilted angle evaporation," Surf. Coat. Tech. (to be published), doi:*10.1016/j.surfcoat.2010.08.131*.

#137336 - $15.00 USD Received 3 Nov 2010; revised 16 Dec 2010; accepted 27 Dec 2010; published 13 Jan 2011

14. M. J. Brett, and M. M. Hawkeye, "Materials science. New materials at a glance," Science **319**(5867), 1192–1193 (2008).
15. J. Q. Xi, M. F. Schubert, J. K. Kim, E. F. Schubert, M. Chen, S. Y. Lin, W. Liu, and J. A. Smart, "Optical thin-film materials with low refractive index for broadband elimination of Fresnel reflection," Nat. Photonics **1**(3), 176–179 (2007).
16. M. F. Schubert, F. W. Mont, S. Chhajed, D. J. Poxson, J. K. Kim, and E. F. Schubert, "Design of multilayer antireflection coatings made from co-sputtered and low-refractive-index materials by genetic algorithm," Opt. Express **16**(8), 5290–5298 (2008).
17. P. Doshi, G. E. Jellison, Jr., and A. Rohatgi, "Characterization and optimization of absorbing plasma-enhanced chemical vapor deposited antireflection coatings for silicon photovoltaics," Appl. Opt. **36**(30), 7826–7837 (1997).
18. E. Spiller, I. Hailer, R. Feder, J. E. E. Baglin, and W. N. Hammer, "Graded-index AR surfaces produced by ion implantation on plastic materials," Appl. Opt. **19**(17), 3022–3026 (1980).
19. P. Yeh, and S. Sari, "Optical properties of stratified media with exponentially graded refractive index," Appl. Opt. **22**(24), 4142–4145 (1983).
20. W. H. Southwell, "Gradient-index antireflection coatings," Opt. Lett. **8**(11), 584–586 (1983).
21. M. Chen, H. C. Chang, A. S. P. Chang, S. Y. Lin, J. Q. Xi, and E. F. Schubert, "Design of optical path for wide-angle gradient-index antireflection coatings," Appl. Opt. **46**(26), 6533–6538 (2007).
22. D. J. Poxson, F. W. Mont, M. F. Schubert, J. K. Kim, and E. F. Schubert, "Quantification of porosity and deposition rate of nanoporous films grown by oblique-angle deposition," Appl. Phys. Lett. **93**(10), 101914 (2008).
23. R. N. Tait, T. Smy, and M. J. Brett, "Modelling and characterization of columnar growth in evaporated films," Thin Solid Films **226**(2), 196–201 (1993).
24. R. Santbergen, J. M. Goud, M. Zeman, J. A. M. van Roosmalen, and R. J. C. van Zolingen, "The AM 1.5 absorption factor of thin-film solar cells," Sol. Energy Mater. Sol. Cells **94**(5), 715–723 (2010).

1. Introduction

Amorphous silicon (a-Si) is a promising photovoltaic material, which is nontoxic, abundant, and has a mature processing technology, allowing cost-effective thin film and flexible devices [1,2]. However, the effective absorption depth of a-Si is only about 1 μm, i.e., 2 orders of magnitude thinner than that of crystalline silicon. On the other hand, minority carriers in the a-Si have very short carrier diffusion length of around 300 nm or less [3]. Hence an efficient light management is essential to improve the device performance of thin film a-Si solar cells.

Usually, a large portion of incident light is reflected back from the surface of a-Si due to the high refractive index of a-Si and thus cannot be used to generate carriers in solar cells. A typical example of reflection-suppressing technique includes the use of surface texturing. However, such large scale texturing causes both the scattering of light into the solar cell and the increase of minority carrier recombination in the surface and junction regions [4]. From the geometrical reason, it is also not suitable for thin film solar cells. Quarter-wavelength dielectric thin films are now the industrial standard for antireflection coatings (ARCs) to increase the light absorption in thin film solar cells. But, this quarter-wavelength ARC is achieved only at a specific wavelength because the films have uniform refractive index throughout the whole film.

In past years, many approaches for fabricating ARCs have been presented to achieve an ideal broadband antireflection property in the visible and near-infrared wavelength range by using graded-refractive-index-structures (GRISs). More than a hundred years have passed since Lord Rayleigh theoretically proposed ARCs with gradient index profiles [5]. Very recently, many research efforts on continuously GRISs have been carried out [6–9]. A continuously varying porosity and effective refractive index of biomimetic nanostructures was obtained by using plasma etching or metal-assistant chemical etching, as well as nanorod arrays. An alternative approach to them is to use the step GRIS [10–12]. Many recent efforts focus on optimization of the discrete refractive index and thickness distribution. The oblique-angle depositions (OAD) of SiO_2/TiO_2, vapor deposition of materials and spin-coated organic materials with different refractive indices have been used to achieve the step GRIS. However, all of the aforementioned techniques employ three-dimensional submicron structures which can cause mechanical and thermal reliability issues. Also, humidity can have impact upon their performance due to the presence of exposed voids. In addition, most importantly few technologies are applicable to the superstrate-type thin film a-Si solar cells using glass

#137336 - $15.00 USD Received 3 Nov 2010; revised 16 Dec 2010; accepted 27 Dec 2010; published 13 Jan 2011

substrate because it covers the surface of active materials and undesirably increases the complexity in the fabrication process.

In this work, we propounded new conceptual AR GRIS for superstrate-type thin film a-Si solar cells. Figure 1 (a) shows the thin film a-Si solar cell structures without and with GRIS. Recently, we have developed low effective refractive index a-Si films deposited by OAD [13]. The OAD is very well-established technique for controlling the optical properties of materials by porosity [14,15]. The effective refractive index of a-Si film can be controlled by the angle of incident flux in e-beam evaporation from the refractive index of a-Si to nearby that of air, and thus it is possible to fabricate the structure having gradually decreasing refractive index. The a-Si GRIS is placed between a-Si (absorptive layer) and indium-tin-oxide (ITO), providing efficient impedance matching through a gradual reduction of the effective refractive index. By suppressing the reflection at the interface between a-Si and ITO, more light can reach the absorptive a-Si layer. Hence the absorption efficiency of thin film a-Si solar cells can be greatly improved over a large range of wavelengths and angles of incidence.

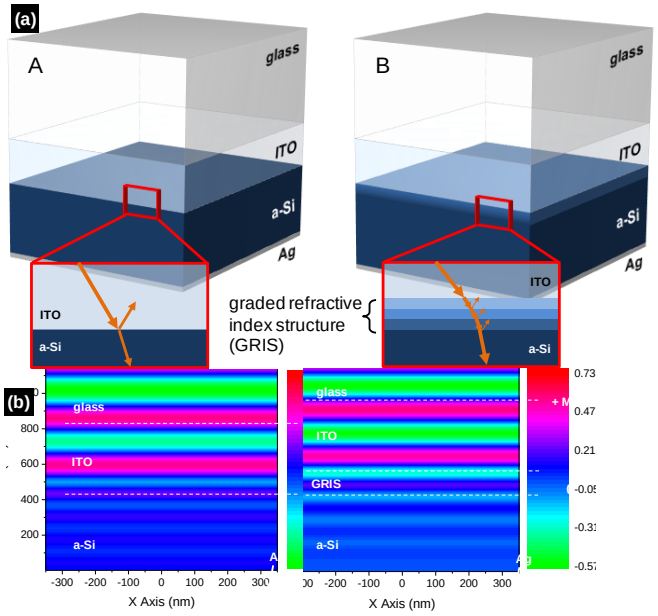

Fig. 1. (a) Schematic diagrams of typical superstrate type thin film solar cell structure (Sample A) and proposed structure with GRIS (Sample B). The magnified images in red squares express the light propagation through the interface between ITO and a-Si layer with and without the GRIS. (b) Electric field distribution in the structures with and without the GRIS.

Figure 1 (a) shows the schematic diagrams of the typical superstrate thin film a-Si solar cell structure (named sample A) and the proposed structure with GRIS (named sample B). In the red squares of Fig. 1 (a), magnified images of each structure are shown for the comparison of light propagation inside the solar cell structures. The red arrows represent the intensity and path of the incident light. In the case of sample A, there exists large index difference between ITO layer and a-Si layer due to the high refractive index of a-Si. While a considerable portion of incident light is reflected from that interface in sample A, most light can be transmitted through the GRIS in sample B due to the grading of the refractive index profile. Figure 1 (b) shows electric field distributions in the solar cell structures with and without GRIS. The large portion of the electric field cannot penetrate the interface between ITO and a-Si layer due to the abrupt change in the refractive index, whereas the electric field can stay in the absorptive layer (a-Si) by the presence of GRIS. The GRIS of sample B consists three different effective refractive index layers with each thickness of 50 nm. The effective refractive index and extinction coefficient of each layer were carefully chosen from last results [13].

#137336 - $15.00 USD Received 3 Nov 2010; revised 16 Dec 2010; accepted 27 Dec 2010; published 13 Jan 2011

2. RCWA simulation of GRIS of a-Si

In order to optimize the gradient refractive index profile, a genetic algorithm would be helpful because there are so many variables which would affect the reflection of the structures [16]. Furthermore, since there is always a trade-off between reflection and absorption in high-*k* (*k* is extinction coefficient) material based ARCs, a careful consideration to the thicknesses and refractive indices of layers must be given [17]. The GRIS can play roles in both ARC and absorptive layer for thin film a-Si solar cells because it is made of a-Si, being placed between ITO layer and a-Si layer. Hence, the thickness of GRIS does not have to be thick, and the number of interfaces in the GRIS should be reduced as many as possible. First, a 150 nm total thickness of the GRIS with three different refractive indices of low-*n* a-Si films was aptly chosen as demonstrated recently [13]. The layer a-Si, which has the highest refractive index and extinction coefficient, was used for an absorptive layer, and G1, G2, G3 layers were employed as three step gradient layers. After each effective refractive index of step layers was chosen properly, their thickness also needs to be determined, by comparing various refractive index profiles according to the thickness distribution in the GRIS. Various refractive index profiles including Gaussian, Exponential, and Quintic have been studied previously [18–20]. The thickness of each layer with four index profiles is shown in Table 1. The effective refractive index for the specific layer was chosen at the wavelength of 600 nm. To calculate the reflectance from the various index profiles, we used a three-dimensional rigorous coupled-wave analysis (RCWA) method. The material properties of a-Si were considered to obtain the exact results at each wavelength by ellipsometry measurements. A plane wave is assumed incident with a fixed polarization angle of 45° instead of a randomly polarized light. For the design and selection of graded index profiles to achieve efficient antireflection over a broadband with a wide range of incident angles, we have theoretically investigated several specific index profiles. Three general profiles and Cubic profile (uniform thickness distribution) were studied, and their governing equations of each profile are given by

$$n(x) = n_{ITO} + (n_{a\text{-}Si} - n_{ITO})x, \tag{1}$$

$$n(x) = n_{ITO} + (n_{a\text{-}Si} - n_{ITO})(10x^3 - 15x^4 + 6x^5), \tag{2}$$

$$n(x) = n_{ITO} + (n_{a\text{-}Si} - n_{ITO})exp\left[-\left(\tfrac{x-1}{0.4}\right)^2\right], \tag{3}$$

$$n(x) = n_{ITO} + (n_{a\text{-}Si} - n_{ITO})(-0.3x^3 + 2.4x^2 - 6.4x + 6.2), \tag{4}$$

where n_{ITO} and $n_{a\text{-}Si}$ are the refractive indices of ITO and a-Si layers, respectively, and x is the thickness of ARC [21].

Table 1. Thickness of 5 layers and their measured refractive indices for different graded index profiles

Layer	Linear	Quintic	Gaussian	Cubic	Effective Refractive Index @600 nm
ITO	400 nm	400 nm	400 nm	400 nm	1.96
G1	14.3 nm	51.9 nm	67.4 nm	50 nm	2.08683
G2	75.8 nm	60.6 nm	56.3 nm	50 nm	2.765
G3	59.9 nm	37.5 nm	26.3 nm	50 nm	3.32532
a-Si	500 nm	500 nm	500 nm	500 nm	3.93551

The reflectance of the structures with four different index profiles was calculated by RCWA method. Since the RCWA simulation includes the interference effects due to the reflection and transmission at each interface of the calculated structure, it is useful to the

#137336 - $15.00 USD Received 3 Nov 2010; revised 16 Dec 2010; accepted 27 Dec 2010; published 13 Jan 2011

theoretical investigation of optical properties of multi-stacked structures. Since the thickness of ITO does not affect the reflectance of solar cell structures, it was set to 400 nm. To get enough absorption, the thickness of a-Si layer was determined as 500 nm, followed by 30 nm thick Ag layer as a back reflector. Figure 2 (a-e) shows the angle dependence of reflectance of four different index profiles. As depicted in Fig. 2 (e), the Cubic index profile is most proper to reduce the reflection from the solar cell structure over the whole incident angle of light and in the wavelength range from 400 nm to 800 nm. It is also noticeable that the lowest reflectance is shown by the Cubic profile of ARC. The Cubic profile exhibits nearly uniform refractive index distribution between ITO layer and a-Si layer.

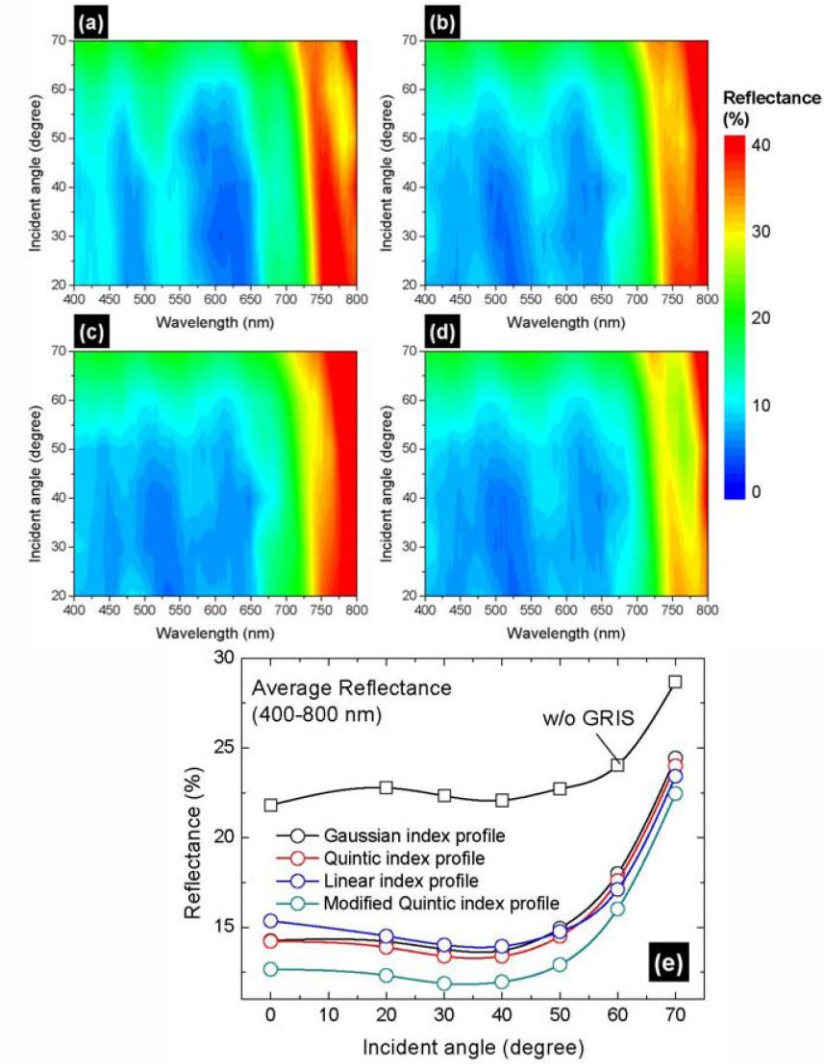

Fig. 2. Calculated reflectance of (a) Linear, (b) Quintic, (c) Gaussian, and (d) Cubic index profiles as function of wavelength in the range of 400-800 nm for incident angles of 20-70°. (e) Calculated average reflectance of various index profiles of the GRIS and of the structure without the GRIS as a function of incident angle of light.

Figure 3 (a) shows the calculated reflectance of both samples A and B as a function of wavelength. For sample A without the GRIS, the reflectance of 5-20% with ripples in the visible range was observed, it is rapidly increased at wavelengths above 700 nm. Generally, the light with longer wavelengths than 800 nm is not absorbed by a-Si, hence most of them

#137336 - $15.00 USD Received 3 Nov 2010; revised 16 Dec 2010; accepted 27 Dec 2010; published 13 Jan 2011

would be transmitted through the a-Si layer, and then be reflected by the back reflector Ag layer. On the contrary, the sample B with the GRIS shows relatively low reflectance of 5-10% with weaker ripples in the visible range compared to the sample A, and the increase of reflectance is slightly low at wavelengths above 700 nm. The ripple pattern in the visible wavelength range is generated mainly by the interference of light at the top and bottom interfaces of ITO layer. The sample B (with GRIS) reduced significantly the reflection and suppressed the ripples in the visible wavelength region. This means that the relatively large amount light can path through the GRIS and then be absorbed by a-Si layer. Because the a-Si GRIS was designed to have a refractive index matching with ITO, the structure with the GRIS (sample B) differed widely from the conventional structure in their reflective properties, thus it can be figured out that its refractive index profile is very applicable to reduce the reflection at the interface of thin film solar cells. Figure 3 (b) shows the designed Cubic graded refractive index profile as a function of layer thickness. The black dot line in the Fig. 3 (b) represents the Cubic polynomial fit.

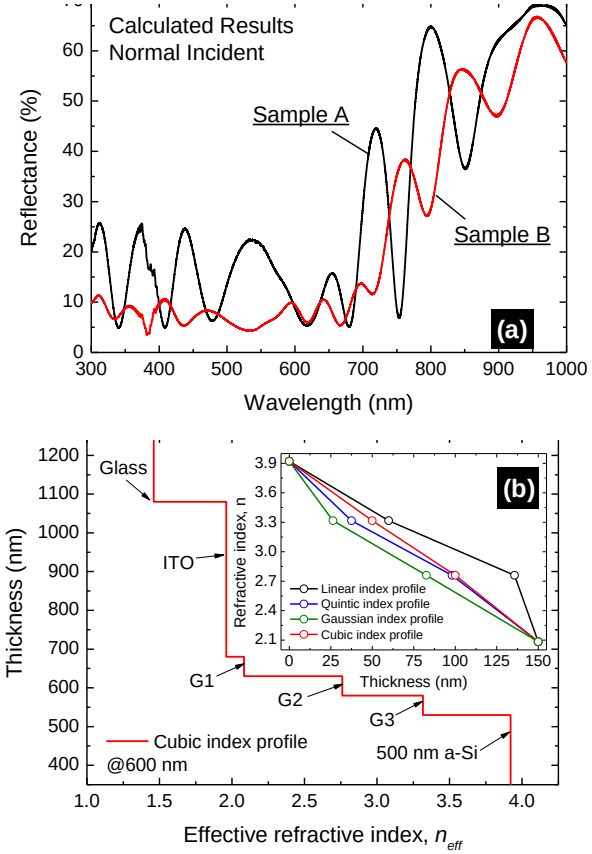

Fig. 3. (a) Calculated reflectance of sample A (without the GRIS) and B (with the GRIS) at normal incidence as a function of wavelength. (b) Effective refractive index profile of the Cubic index profile as a function of thickness. The effective refractive index is chosen at the wavelength of 600 nm.

3. Fabrication of thin film a-Si solar cell structure

In order to demonstrate the proposed structure, the samples A and B were fabricated on the glass substrate by e-beam evaporation. Figure 4 (a) and (b) show the cross-sectional SEM images of fabricated thin film a-Si solar cell structures without and with Cubic GRIS, respectively. The 400 nm thick ITO layer was deposited on glass by e-beam evaporation, and

#137336 - $15.00 USD Received 3 Nov 2010; revised 16 Dec 2010; accepted 27 Dec 2010; published 13 Jan 2011

annealed by rapid thermal annealing process at 500 °C for 2 min. After the ITO layer becomes transparent, the a-Si layer was deposited with three different steps varying the angle of incidence of e-beam flux. First, the lowest effective refractive index layer was deposited with the tilted angle of 70°, and then the angles were changed step by step 50° and 35° for each G2 and G3 layer, respectively. For achieving the Cubic GRIS, 50 nm-thick film was deposited for each G1, G2, and G3 layers with very small variation of thickness. Finally, the 500 nm thick a-Si layer as the absorptive layer was deposited without tilting, followed by the deposition of 30 nm thick Ag layer as a back reflector. For all the evaporation of a-Si, the deposition rate was fixed at 1 nm/s, and the deposition rate of ITO and Ag was 0.2 nm/s and 0.1 nm/s, respectively. As shown in magnified field-emission transmission electron microscope (FE-TEM) image of the GRIS in the inset of Fig. 4 (a), the oblique nanocolumnar structure is caused by the self-shadowing effect during the OAD. The initially evaporated Si islands prevent the following incident flux from reaching the shadow regions, thus producing the porous films constituted of nanoscale columns or nanorods [22]. As depicted in the inset of Fig. 4 (a), the angle of nanocolumns is slightly varied from the ITO interface to the a-Si layer interface because the incident angle of e-beam flux is changed from 70° to 35°. For the incident flux angles (θ_{tilt}) of 70°, 50°, and 35°, the deposited a-Si nanocolumn angles of θ_{Si1} = 51°, θ_{Si2} = 29°, and θ_{Si3} = 16° were measured, respectively. The θ_{tilt} does not precisely match the θ_{Si} in the porous Si film, and is typically larger than the θ_{Si}. The empirical relations between these two angles are given by the tangent rule of $\tan\theta_{Si} = (\tan\theta_{tilt})/2$ for small θ_{tilt} and the cosine rule of $\theta_{Si} = \theta_{tilt} - \sin^{-1}\left[(1-\cos\theta_{tilt})/2\right]$ for large θ_{Si} [23]. The discrepancy between the theoretical and experimental results may be caused by variations in the deposition parameters including deposition rate, chamber pressure, and substrate temperature, and that is shown in Fig. 5.

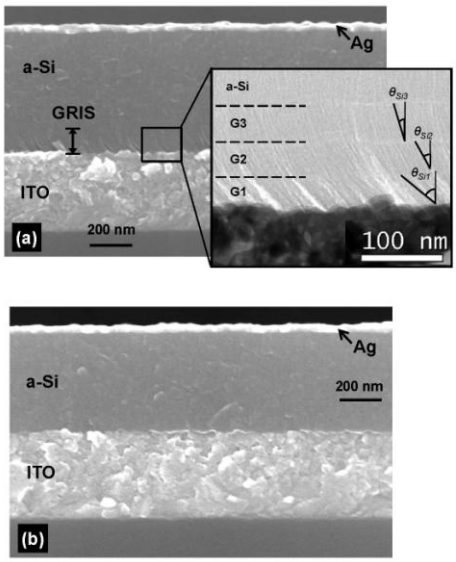

Fig. 4. SEM image of the structure (a) with and (b) without the GRIS. The inset of (a) is a TEM image of the GRIS. The magnified TEM image shows the distinct nanocolumnar structure of GRIS.

#137336 - $15.00 USD Received 3 Nov 2010; revised 16 Dec 2010; accepted 27 Dec 2010; published 13 Jan 2011

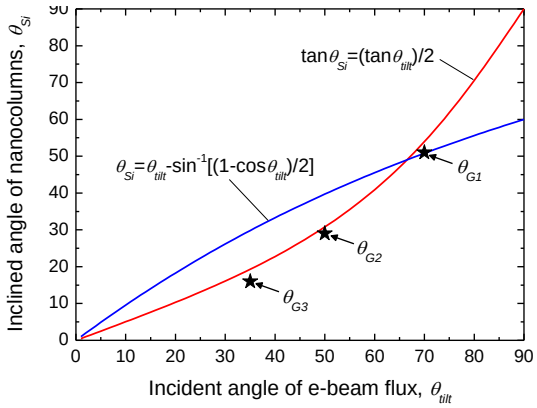

Fig. 5. Tangent rule and Cosine rule between the incident angle of e-beam flux and the inclined angle of nanocolumnar structure. The star marks indicate the experimental points of each layer of the GRIS.

4. Results and Discussion

To characterize the effect of the GRIS on the antireflection property, spectrophotometry measurements were conducted. The reflectance was measured over a broad wavelength range from 300 nm to 1000 nm including the major absorptive wavelength range of a-Si from 400 nm to 800 nm [24]. The measured reflectance spectra of both samples under normal incidence are shown in Fig. 6. The measured reflectance is roughly consistent with the calculated result in the visible range. The slightly low reflectance and magnitude of ripple pattern of both samples in the wavelength range of UV and IR may be attributed to the difference between the optical properties of a-Si single layer and that of the a-Si layers of thin film solar cell structure. There is little difference in the ripple pattern of reflectance between the measured and calculated results in the UV and visible wavelength region, however in IR wavelength region the magnitude of ripple pattern of sample B (with GRIS) is remarkably reduced when it was compared with sample A (without GRIS) for both measured and calculated results. This may be caused by the GRIS because the light reflected from Ag is not reflected as much as that of sample A. However, for the a-Si solar cells, strong absorption of a-Si occurs in the visible wavelength range. The GRIS is directly contributed to the suppression of reflectance of the thin film a-Si solar cell structure.

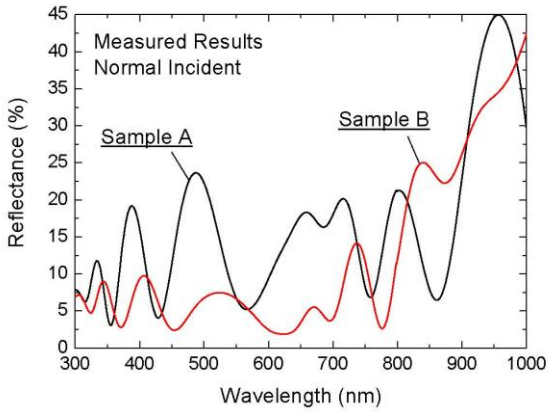

Fig. 6. Measured reflectance of sample A (without the GRIS) and B (with the GRIS) at normal incidence as a function of wavelength.

#137336 - $15.00 USD Received 3 Nov 2010; revised 16 Dec 2010; accepted 27 Dec 2010; published 13 Jan 2011

Figure 7 (a) and (b) show the calculated reflectance and Fig. 7 (c) and (d) show the measured reflectance as function of incident angle and wavelength. As can be seen in both the calculated and measured results, the reflection from the solar cell structure is suppressed significantly by the use of the GRIS between ITO and a-Si layer. Despite of a little discreapancy between calculated and measured results, it is obvious that the significant decrease of reflection by GRIS is present. Figure 8 shows the measured average reflectance depending on the angle of incidence. The measured reflectance at each incident angle of light was averaged in the wavelength range from 400 nm to 800 nm. The incident angle dependent reflectance was measured by spectrophotometer with a depolarizer to give unpolarized light. The measured average reflectance is slightly increased as the angle of incidence becomes larger from normal, and above 40° of incident angle it is rapidly increased for both samples. In the incident angle range of 0-50°, which is especially important for practical solar cell applications, the average reflectance was less than 10% at wavelengths of 400-800 nm. The experimental results are in reasonable agreement with the calculated results, and the difference between reflectances of the solar cell structures with and without the GRIS is also about 10%. Furthermore the interference oscillations are greatly reduced in the reflectance spectrum of sample B. This can be explained by the fact that light is mostly absorbed after reflection by the Ag, indicating an improved more light arrival by effective refractive index matching. At normal incidence, the average reflectance of the solar cell structure with the GRIS was decreased by 54%. Consequently, the use of the GRIS in the thin film a-Si solar cells, which is very simple and low cost, provides efficient wide-angle antireflection properties.

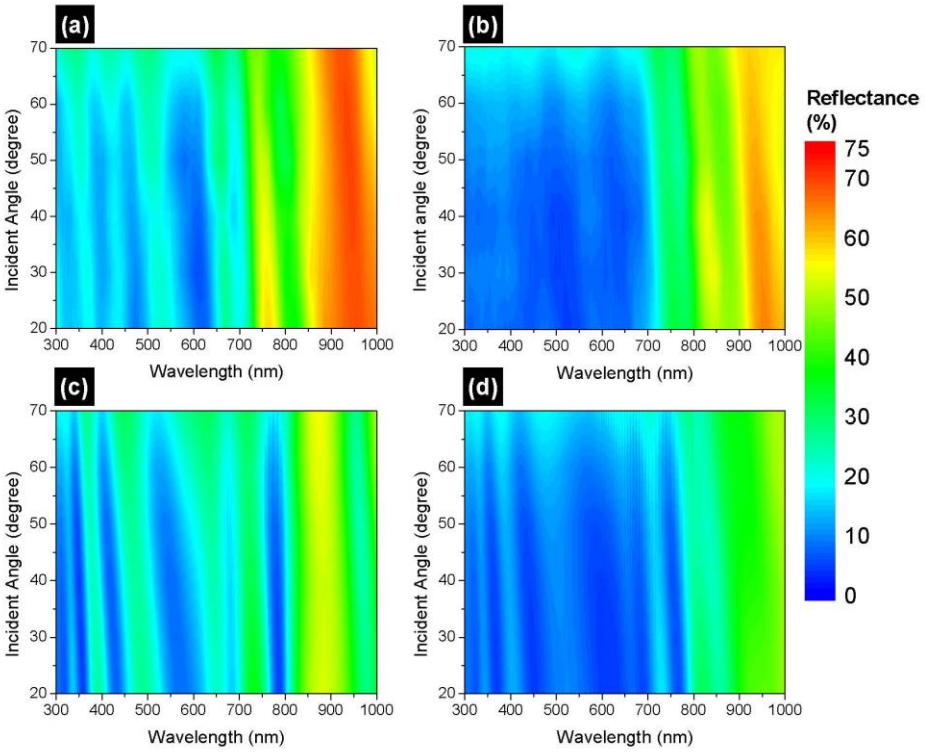

Fig. 7. Calculated reflectance of the structures (a) without and (b) with the GRIS as function of wavelength and incident angle. Measured reflectance of the structures (c) without and (d) with the GRIS as function of wavelength and incident angle.

#137336 - $15.00 USD Received 3 Nov 2010; revised 16 Dec 2010; accepted 27 Dec 2010; published 13 Jan 2011

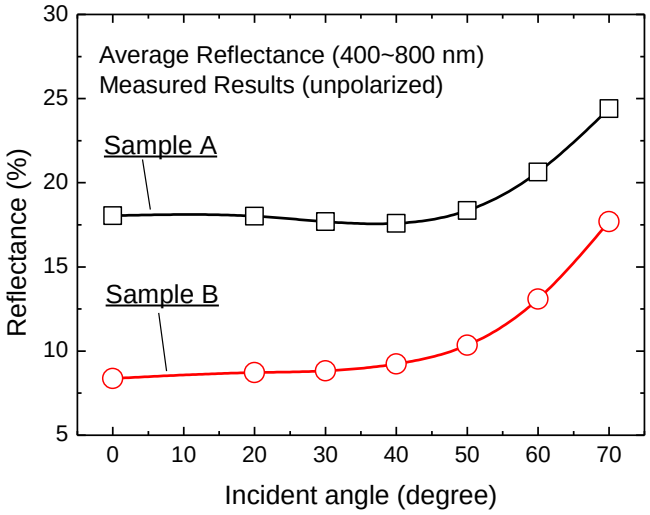

Fig. 8. Measured average reflectance of sample A and B as a function of incident angle for unpolarized light.

5. Conclusion

In summary, the novel thin film a-Si solar cell structure with GRIS was proposed for suppressing the reflectance at the interface between ITO layer and a-Si layer. The antireflective GRIS which has the refractive index matched to the ITO layer is placed on the absorptive layer, thus reducing the reflection from that interface mentioned above. The optical property of the structure was investigated theoretically and experimentally, and the calculated results in reasonable agreement with the measured results. The GRIS was fabricated by e-beam evaporation with OAD technique, hence the effective refractive index of a-Si can be varied controllably by angle of incident e-beam flux. The reflectance of solar cell structure with the GRIS is suppressed over the whole desired wavelength range, and its average value in the wavelength range 400-800 nm was decreased by 54% from the conventional solar cell structure without the GRIS. Compared to other antireflective structures, the structure with the GRIS of a-Si is more promising for the enhancement of efficiency of superstrate type thin film a-Si solar cells.

Acknowledgements

This work was supported by the Core Technology Development Program for Next-generation Solar Cells of Research Institute for Solar and Sustainable Energies (RISE), GIST and by the WCU program of MEST (Project No. R31-2008-000-10026-0).

#137336 - $15.00 USD Received 3 Nov 2010; revised 16 Dec 2010; accepted 27 Dec 2010; published 13 Jan 2011